

# Ancient Medicinal Insect *Steleophaga Plancyi* (Boleny)-Derived Extracellular Vesicle-Like Particles Enhances Autophagic Activity to Promote Osteogenic Differentiation via Melatonin in Osteoporosis

Jiaxu Lu<sup>1,2,\*</sup>, Jiaxian Chen<sup>2,\*</sup>, Youping Jiang<sup>1,2</sup>, Yuanyuan Liu<sup>1,2</sup>, Sheng Yu<sup>2</sup>, Zhen Shi<sup>2</sup>, Peicong Chen<sup>2</sup>, Hao Lin<sup>2</sup>, Peng Li<sup>1,2</sup> 

<sup>1</sup>Stem Cell Research and Cellular Therapy Center, Affiliated Hospital of Guangdong Medical University, Zhanjiang, 524001, People's Republic of China;

<sup>2</sup>Orthopedic Center, Affiliated Hospital of Guangdong Medical University, Zhanjiang, 524001, People's Republic of China

\*These authors contributed equally to this work

Correspondence: Hao Lin, Orthopedic Center, Affiliated Hospital of Guangdong Medical University, Zhanjiang, 524001, People's Republic of China, Email [linhao@gdmu.edu.cn](mailto:linhao@gdmu.edu.cn); Peng Li, Stem Cell Research and Cellular Therapy Center, Affiliated Hospital of Guangdong Medical University, Zhanjiang, 524001, People's Republic of China, Email [13763086273@163.com](mailto:13763086273@163.com)

**Introduction:** Osteoporosis, a critical public health challenge, is marked by skeletal deformities and heightened fracture risk. *Steleophaga plancyi* (Boleny) (SP), a component of traditional Chinese medicine, is known to enhance bone health, but the molecular mechanisms behind its osteoprotective effects are not well understood.

**Methods:** We isolated extracellular vesicle (EV)-like particles from SP (SP-EVLP) using differential velocity centrifugation and investigated their effects on human bone marrow stromal cells (hBMSCs) in vitro. We utilized CCK-8, Alkaline phosphatase (ALP) and alizarin red staining (ARS), RNA-seq, bioinformatics, immunofluorescence, and Western blot to elucidate the osteoprotective role and mechanisms of SP-EVLP. The therapeutic potential of SP-EVLP was evaluated in an ovariectomized (OVX) rat model, a standard model for osteoporosis, by encapsulating them in enteric-coated capsules.

**Results:** SP-EVLP were successfully isolated and characterized, and they were shown to be effectively internalized by hBMSCs, enhancing osteogenic differentiation. In the OVX rat model, SP-EVLP encapsulated in enteric-coated capsules significantly increased bone mass, indicating a robust osteoprotective effect. Further mechanistic studies revealed that SP-EVLP promotes osteoblast proliferation by activating melatonin-induced autophagy, a pathway that may improve osteoporotic conditions.

**Conclusion:** Our results establish SP-EVLP as a promising therapeutic candidate for osteoporosis. The activation of melatonin-induced autophagy by SP-EVLP suggests a molecular mechanism for its osteoprotective effects, opening new possibilities for osteoporosis treatment development.

**Keywords:** Osteoporosis, *Steleophaga plancyi* (Boleny), extracellular vesicles (EV)-like particles, autophagy, melatonin

## Introduction

Osteoporosis, an insidious degenerative condition, is defined by increased bone resorption and diminished bone tissue microarchitecture, predisposing individuals to fractures.<sup>1</sup> Spine or hip fractures, the most common complications of osteoporosis, exacerbating elder patient morbidity and mortality.<sup>2</sup> Epidemiological studies indicate that osteoporosis affects one in three women and one in five men over 50 years of age.<sup>3</sup> Bone formation is closely correlated to the osteogenic differentiation of mesenchymal stem cells (MSCs), which highlights the critical role of MSC osteogenic differentiation in osteoporosis treatment.<sup>4</sup>

Current osteoporosis treatments, including hormone therapy, bisphosphonates, and raloxifene, often come with long-term side effects such as increased cardiovascular risks, as well as significant economic burdens.<sup>5</sup> This has led to a growing interest in herbal interventions as alternative approaches for osteoporosis management. A comprehensive review of clinical trials has shown that plant-derived medicines, including those from *Acanthopanax senticosus*, *Actaea racemosa*, and *Camellia sinensis*, have demonstrated promising results in targeting various pathways in bone metabolism, anti-inflammatory, antioxidant, and estrogen-like functions. These natural products may offer a safer and more cost-effective strategy for enhancing patient outcomes without the side effects associated with conventional therapies.<sup>6</sup> However, further studies are needed to confirm the effectiveness and safety of these herbal medicines.

Exosomes, nanoscale extracellular vesicles (30–120 nm), contains a diverse of bioactive molecules, including lipids, proteins, and nucleic acids.<sup>7</sup> Emerging evidence highlights the therapeutic potential of exosomes in treating various diseases, such as antitumor activity,<sup>8</sup> tissue regeneration,<sup>9</sup> and anti-inflammation.<sup>10</sup> Jin-Hyeon Hwang et al demonstrated that exosome-like nanovesicles from yams enhance osteoblast differentiation and mineralization, thereby promoting bone regeneration.<sup>11</sup> Similarly, our earlier research indicated that *Pueraria lobata*-derived exosome-like nanovesicles stimulate autophagy, leading to the degradation of TMAO and subsequent promotion of human bone mesenchymal stem cells (hBMSCs) differentiation and mineralization.<sup>12</sup> Collectively, these findings suggest that exosomes isolated from natural products could represent a novel therapeutic strategy for osteoporosis management.<sup>13</sup>

The intricate molecular interplay between autophagy and EVs is multifaceted. Autophagy-related proteins (ATGs) are instrumental in EV biogenesis, indicating a shared molecular foundation between these processes. EVs can modulate autophagy in recipient cells by delivering signaling molecules, thus contributing to cellular homeostasis through lysosomal degradation and extracellular molecule secretion.<sup>14</sup> Microglial EVs have been demonstrated to regulate biological pathways and activate autophagy, ensuring microglial survival and homeostasis.<sup>15</sup> This bidirectional regulation forms a dynamic feedback loop, where EVs can either activate or inhibit autophagy, and autophagy, in turn, influences EV production.<sup>16</sup> In the context of cardiovascular diseases, the interplay between EVs and autophagy is crucial in disease pathophysiology, offering potential therapeutic targets.<sup>17</sup> However, the molecular mechanisms behind the osteoprotective effects between autophagy and EVs are not well understood.

Insects have been integral to traditional Chinese medicine, with *Steleophaga plancyi* (Boleny) (SP) noted for its therapeutic applications since the “Shen Nong Ben Cao Jing” era, circa 3rd century AD.<sup>18</sup> SP is recognized for its role in treating a spectrum of conditions including bone diseases, trauma, gynecological issues, and diabetes.<sup>19</sup> Research has shown that SP can stimulate the healing of bone fractures, potentially through the increase of bone morphogenetic proteins (BMPs) and vascular endothelial growth factor (VEGF).<sup>20</sup> Despite these traditional applications, the active constituents in SP responsible for these effects remain to be fully elucidated.

In this study, we successfully isolated EV-like particles (EVLP) from SP, which displayed typical exosomal morphology and particle size. Co-culture experiments with human bone marrow stromal cells (hBMSCs) demonstrated that SP-EVLP were internalized and enhanced osteogenic differentiation. Furthermore, SP-EVLP treatment ameliorated bone loss in an OVX rat model. Mechanistically, SP-EVLP activated autophagy via melatonin, potentially mitigating osteoporotic progression. Our findings suggest the therapeutic potential of SP-EVLP in osteoporosis management.

## Materials and Methods

### Isolation and Characterization of SP-EVLP

SP-EVLP were isolated via differential velocity centrifugation. Briefly, SP powder was suspended in PBS (w/v, 1:2 to 1:4) at 26 °C for 24 hours. The supernatant was centrifuged at 2,500×g for 30 minutes and 10,000×g for 1 hour to eliminate impurities and cell debris. Ultracentrifugation at 108,000×g for 1.5 hours was then performed to pellet the SP-EVLP. The pellet was resuspended in PBS and stored at –80 °C for subsequent analysis. The zeta potential of SP-EVLP was determined using a ZetaSizer Pro (Malvern), while particle size was assessed by nanoparticle tracking analysis (NTA). Morphological characterization was conducted using transmission electron microscopy (JEM-1400, JEOL Ltd).

## Lipidomic and Metabolomic Analyses of SP-EVLP

Lipidomic and metabolomic profiling of SP-EVLP was performed by Beijing Bio-Tech Pack Technology Company Ltd. Utilizing a LC-MS/MS platform, we conducted a comprehensive quantitative analysis to characterize the lipidome and identify metabolites present in SP-EVLP.

## Cell Culture

hBMSCs were purchased from OriCell<sup>®</sup> Company (Cyagen Biosciences, Guangzhou, China) and cultured in  $\alpha$ -MEM supplemented with 10% fetal bovine serum (FBS, Gibco, USA) and Penicillin-Streptomycin solution (100 IU/mL and 100  $\mu$ g/mL, respectively) at 37°C in a 5% CO<sub>2</sub> atmosphere. After an initial 3-day culture period, hBMSCs were detached and passaged. The culture medium was refreshed every three days.

## ALP Staining

hBMSCs were cultured in 24-well plates with osteogenic induction medium (OIM, 50  $\mu$ M ascorbate-2-phosphate, 100 nM dexamethasone and 10 mm  $\beta$ -glycerophosphate) supplemented with SP-EVLP for 3 days, followed by fixation in 4% paraformaldehyde for 30 minutes. Alkaline phosphatase (ALP) activity was assessed using the BCIP/NBT ALP Color Development Kit (Leagene, Beijing, China), and the stained cells were documented using a microscope (Olympus, Japan).

## ARS Staining

hBMSCs were cultured in 24-well plates with osteogenic induction medium containing SP-EVLP for 14 days, followed by fixation in 4% paraformaldehyde for 30 minutes. Cells were then incubated with Alizarin Red S solution (OriCell, Cyagen Biosciences, Guangzhou, China) for 30 minutes at room temperature. The stained cells were documented using a microscope (Olympus, Japan).

## Cell Proliferation and Viability Measurement

The EdU cell proliferation kit (Beyotime, China) was utilized to assess hBMSCs proliferation. Cells were treated with SP-EVLP for 36 hours, followed by an 18-hour incubation with EdU. Subsequent fixation with 4% paraformaldehyde for 30 minutes was performed, after which cells were processed according to the manufacturer's protocol. Proliferation was analyzed using confocal laser scanning microscopy.

Cell viability was evaluated using the Cell Counting Kit-8 (Zeta life, USA) according to the manufacturer's instructions. hBMSCs were treated with SP-EVLP for 24 h and 72 h, and after the addition of 10  $\mu$ L CCK-8 solution, the cells were incubated for another 1 hour. The absorbance was then measured at 450 nm using a microplate reader (Bio-Rad, USA).

## Extracellular Vesicles-Like Particles Uptake

To visualize the internalization of SP-EVLP by hBMSCs, PKH26-red fluorescent dye (Sigma-Aldrich, USA) was used to label SP-EVLP. Cells were incubated with the labeled SP-EVLP for 2 hours, fixed with 4% paraformaldehyde for 15 minutes, and nuclei were counterstained with DAPI. Internalization was examined using a confocal laser scanning microscopy (Olympus, Japan).

## RNA Sequencing and Data Analysis

hBMSCs induced by OIM were treated with SP-EVLP or PBS, and RNA samples were prepared accordingly. High-throughput sequencing and subsequent bioinformatic analyses were conducted by Allwegene Technology Co., Ltd (Beijing, China) using the Illumina Novaseq 6000 platform. Differential expression was determined for genes with an adjusted P value < 0.05 and  $|\log_2(\text{fold change})| \geq 1$ .<sup>21</sup> Furthermore, Gene Ontology (GO) and KEGG pathway enrichment analyses were applied to categorize the functions of the differentially expressed genes.

## Immunofluorescence Assay

hBMSCs were plated on 12-well plates with coverslips and treated with OIM supplemented with SP-EVLP for 72 hours. Cells were fixed in 4% paraformaldehyde for 15 minutes and permeabilized in 0.1% Triton X-100 for 30 minutes. After blocking with 1% bovine serum albumin for 1 hour, cells were incubated with primary antibodies overnight. Following three washes with PBS, cells were incubated with secondary antibodies, and nuclei were counterstained with DAPI. Fluorescent imaging was performed using a confocal laser scanning microscopy (Olympus, Japan).

## Western Blotting

hBMSCs were lysed in RIPA buffer (Beyotime, China) containing protease and phosphatase inhibitors (Roche, Germany) for 30 minutes on the ice. Then total protein extracts were normalized and separated by SDS-PAGE gel, transferred to PVDF membranes (Millipore, USA) and blocked with 5% milk for 1 hour. Membranes were incubated with primary antibodies at 4 °C overnight: anti-ALP (1:1000), anti-RUNX2 (1:1000), anti-ATG3/7 (1:1000), anti-LC3 I/II (1:1000), and anti- $\beta$ -actin (1:1000) (all purchased from Cell Signaling Technology, USA). After being washed with TBST for 3 times, the membranes were incubated with IgG polyclonal secondary antibodies (Cell Signaling Technology, USA) for 1 hour at room temperature. Finally, the protein expression was determined by enhanced chemiluminescence (ECL) (Bio-Rad, USA) with a ChemiDoc XRS (Bio-Rad, USA).

## In Vivo Experiment

Ten-week-old female SD rats were sourced from the Laboratory Animal Center at the Affiliated Hospital of Guangdong Medical University, with experimental protocols approved by the institution's Ethics Committee on Animal Experiments. Ovariectomy was conducted to establish an osteoporosis model,<sup>12,21–23</sup> and SP-EVLP were encapsulated in enteric-coated capsules supplied by Shanghai Yuyan Instruments Co., Ltd (China). Animals were randomly assigned to four groups (n=5): a control (non-ovariectomized), OVX, OVX with empty capsules, and OVX with SP-EVLP-loaded capsules (10 mg/kg).<sup>11,12</sup> The head of the capsule was unscrewed, and 5  $\mu$ L of SP-EVLP suspension (200 mg/mL) was introduced into the capsule. The treatments were administered intragastrically every three days for a total of 8 weeks.<sup>11</sup> The femurs were scanned using a SCANCO vivaCT80 micro-computed tomography system (pixel size 8.82 mm, operating voltage 80 kV, current 500 mA, exposure time 1500 ms). The 3D model images of the trabecular and cortical bone were reconstructed using CTan software. A total of 120 slices were evaluated, with each voxel sized at 15.6  $\mu$ m. Bone mineral density (BMD), bone volume/total volume (BV/TV), trabecular number (Tb.N) and trabecular thickness (Tb.Th) were assessed using an Inveon Research Workplace (Siemens) as previously described.<sup>12,24</sup> The bone marrow cavity of femurs was flushed with phosphate-buffered saline (PBS), and the suspension was then subjected to centrifugation. These cells were subsequently seeded into a culture flask containing  $\alpha$ -MEM supplemented with 10% FBS (Gibco, USA) and Penicillin-Streptomycin solution (100 IU/mL and 100  $\mu$ g/mL, respectively). On the third day post-seeding, the medium was changed and the cells cultured to facilitate further experiments.

## In Vivo Small Animal Imaging Assay

SP-EVLP were labeled with DIR Far-red Plasma Membrane Fluorescent Probe (Beyotime, 10  $\mu$ M) for 20 minutes at 37°C, followed by centrifugation at 100,000  $\times$  g for 70 minutes in a microcentrifuge to pellet the labeled SP-EVLP.<sup>25,26</sup> The supernatant was then removed, and the pellet was resuspended in PBS for injection into rat via the intraperitoneal route. The in vivo distribution of SP-EVLP within the liver, heart, intestinal, kidney, and femur was subsequently imaged using the Xtreme optical multimodal imaging system (Bruker, Switzerland).

## Histology Analysis

Femoral sections from SD rats were fixed in 4% paraformaldehyde, decalcified using a 10% EDTA, paraffin-embedded, and dehydrated through a series of dimethylbenzene and graded ethanol washes. After washing in TBS, antigen retrieval was performed using a rapid antigen repair solution (Beyotime, China). For immunohistochemical analysis, sections were blocked with 5% BSA for 30 minutes and then incubated with primary antibodies at 4 °C overnight. This was followed

by incubation with streptavidin-conjugated secondary antibodies at room temperature for 45 minutes, and visualization with 3,3'-diaminobenzidine (DAB) (ZSGB-Bio, China). Counterstaining with hematoxylin was performed, and images were captured using a light microscope (Olympus, Japan). Additionally, femurs were stained with H&E and Masson's trichrome staining (Solarbio, China) according to the manufacturer's instructions.

## Statistical Analysis

Data analysis was conducted using GraphPad Prism 8.0 software, with results presented as the mean  $\pm$  SD from three independent replicates. For comparisons involving multiple groups, one-way or two-way ANOVA was employed. A significance level of  $*P < 0.05$  was established.

## Results

### Characterization of SP-EVLP

Transmission electron microscopy (TEM) images demonstrated that SP-EVLP exhibit a cup shaped structure with a lipid bilayer membrane (Figure 1A). Nanoparticle tracking analysis (NTA) revealed a primary particle size peak of approximately 89 nm (Figure 1B). Ponceau S staining and agarose gel electrophoresis confirmed the presence of abundant biological macromolecules, including proteins and nucleic acids, within the SP-EVLP (Figure 1C and D). Additionally, lipidomic analysis indicated that the predominant lipid types in SP-EVLP were PG and Ether-PE (Figure 1E). The average zeta potential and polydispersity index of SP-EVLP were measured at  $-9.707$  mV and 0.213, respectively (Figure 1F). Notably, SP-EVLP were successfully isolated and the characterized.

### SP-EVLP Promoted the Proliferation and Osteogenic Differentiation of hBMSCs

PKH26-labeled SP-EVLP were used to trace their internalization by hBMSCs, as evidenced by red fluorescence surrounding the nuclei (Figure 2A). The CCK8 assay showed that SP-EVLP treatment significantly increased

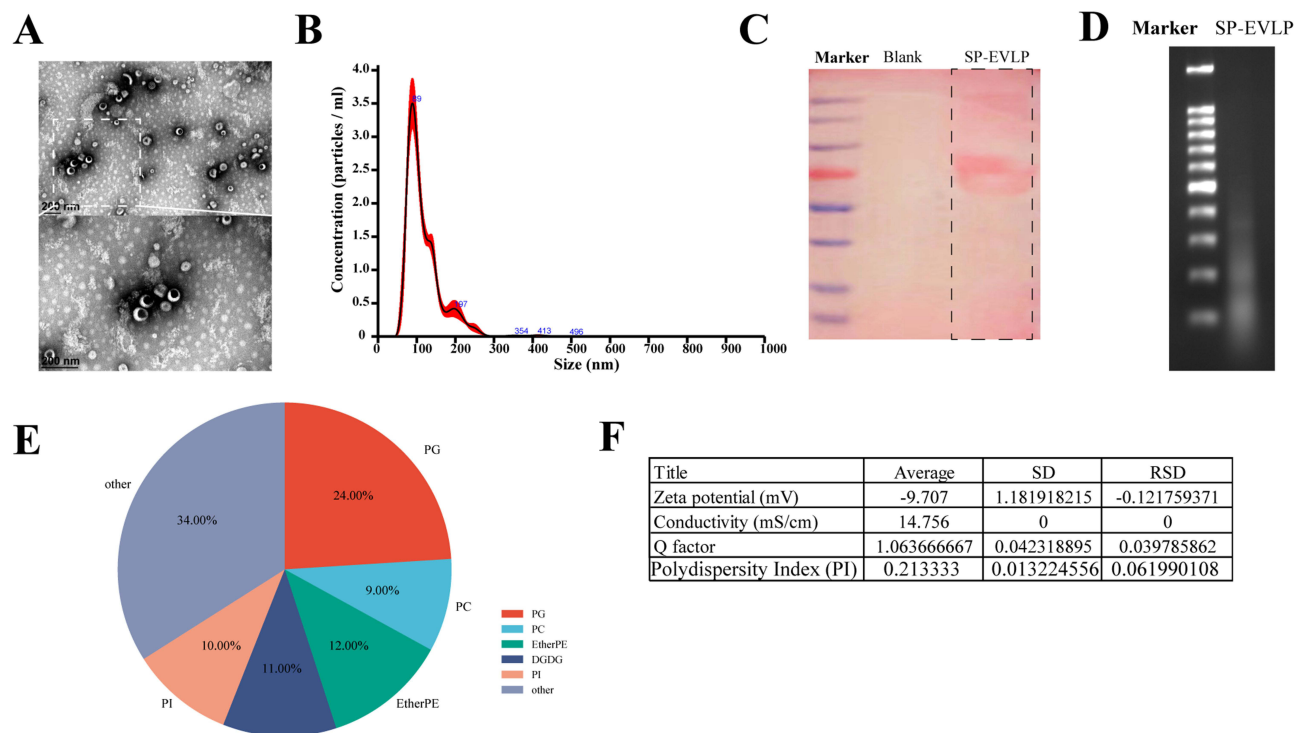


**Figure 1** Characterization of SP-EVLP. **(A)** The structural morphology of the SP-EVLP was examined using TEM. **(B)** The hydrodynamic size distribution and size measurements of the SP-EVLP were determined by NTA. **(C)** The presence of protein within the SP-EVLP were assessed through polyacrylamide gel electrophoresis. **(D)** The nucleic acid of SP-EVLP were characterized by agarose gel electrophoresis. **(E)** Lipids metabolomics of SP-EVLP were elucidated using a LC-MS/MS platform. **(F)** The average zeta potential and polydispersity index of SP-EVLP were characterized using a nanoparticle size and zeta potential analyzer.

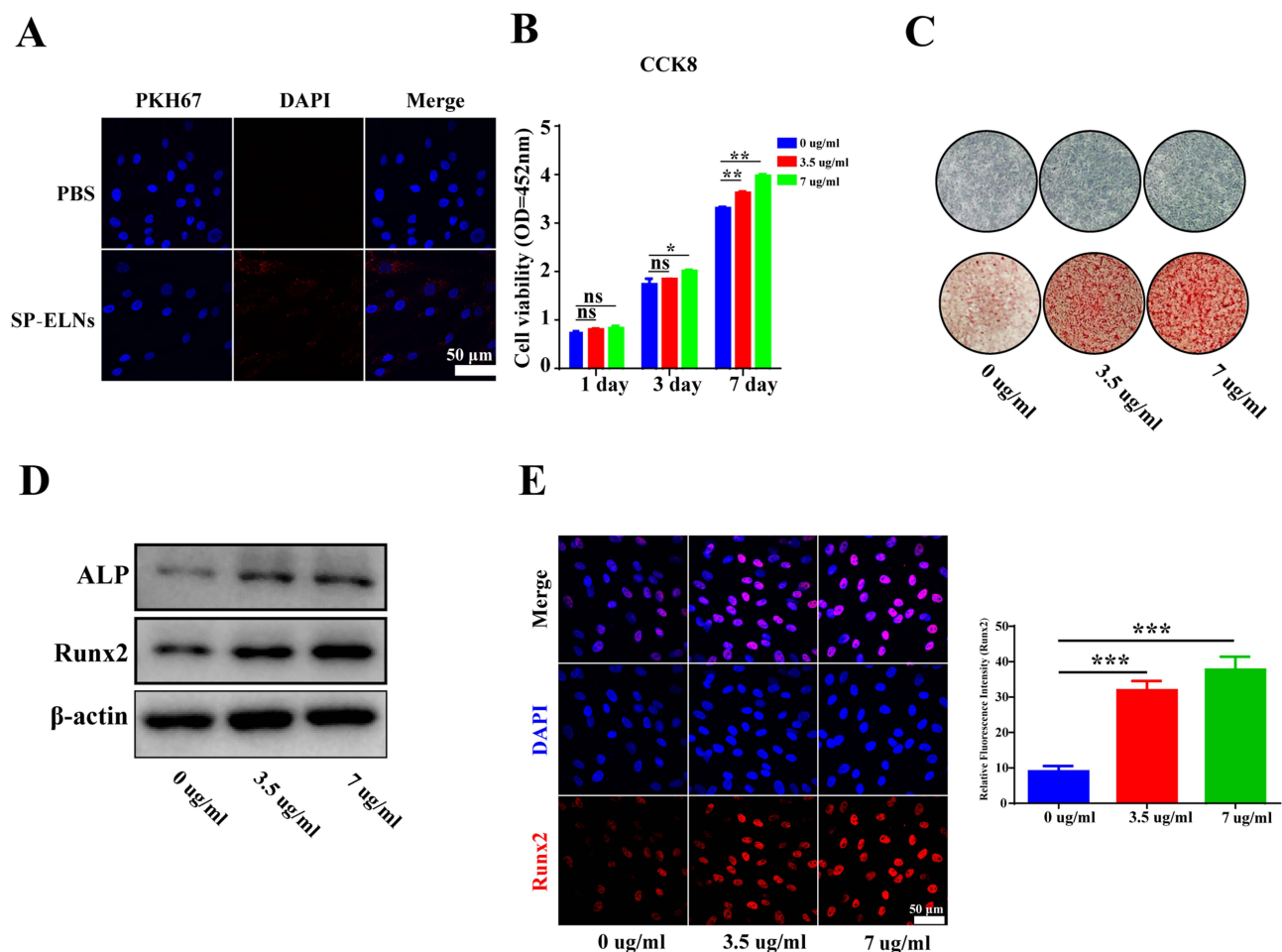


**Figure 2** SP-EVLP promoted the proliferation and osteogenic differentiation of hBMSCs. (A) Confocal microscopy was utilized to visualize the internalization of PKH26-labeled SP-EVLP (red) by hBMSCs, with nuclei counterstained using DAPI (blue). (B) The viability of hBMSCs following incubation with SP-EVLP for 1, 3, and 7 days was assessed using the CCK-8 assay. (C) ALP activity and ARS staining were employed to evaluate the osteogenic differentiation of hBMSCs cultured with varying concentrations of SP-EVLP (0, 3.5, and 7 µg/mL) for 3 and 14 days, respectively. (D) Western blot analysis was conducted to quantify the expression levels of osteogenic markers, including ALP and RUNX2. (E) Fluorescence imaging was used to examine the intracellular localization of RUNX2 (red) in hBMSCs treated with different concentrations of SP-EVLP (0, 3.5, and 7 µg/mL), with nuclei stained by DAPI (blue). Data represent means  $\pm$  SD at least 3 separate experiments. \* $P < 0.05$ , \*\* $P < 0.01$ , and \*\*\* $P < 0.001$ .

hBMSCs proliferation at concentrations of 0, 3.5, and 7 µg/mL over 1, 3, and 7 days (Figure 2B). Osteogenic differentiation was induced by SP-EVLP in osteogenic medium, leading to elevated ALP activity (Figure 2C, down) and increased calcium salt deposition as shown by ARS staining (Figure 2C, up), indicating enhanced mineralization and early osteogenic marker expression. Western blotting confirmed increased protein levels of ALP and RUNX2, key osteogenic markers,<sup>27</sup> in response to SP-EVLP treatment (Figure 2D). Immunofluorescence also revealed increased nuclear RUNX2 expression, further supporting the osteogenic commitment induced by SP-EVLP (Figure 2E). These results collectively indicate that SP-EVLP promote both proliferation and osteogenic differentiation in hBMSCs.

### SP-EVLP Promoted Cell Cycle and Autophagy

RNA sequencing coupled with GO and KEGG analyses uncovered 3,333 differentially expressed mRNAs in SP-EVLP-treated hBMSCs compared to negative controls, comprising 1,351 downregulated and 1,982 upregulated genes (Figure 3A). KEGG analysis indicated substantial activation of mitophagy and autophagy-related pathways, and GO analysis underscored the role of SP-EVLP in cell developmental processes (Figure 3B and C). Western blotting showed elevated cyclin D1 levels, a regulator of G1-to-S transition (Figure 3D). In addition, flow cytometry analysis demonstrated that SP-EVLP facilitate S phase cell cycle progression (Figure 3E). Collectively, these findings indicate that SP-EVLP enhance hBMSC proliferation by modulating cell cycle advancement. Western blotting also confirmed

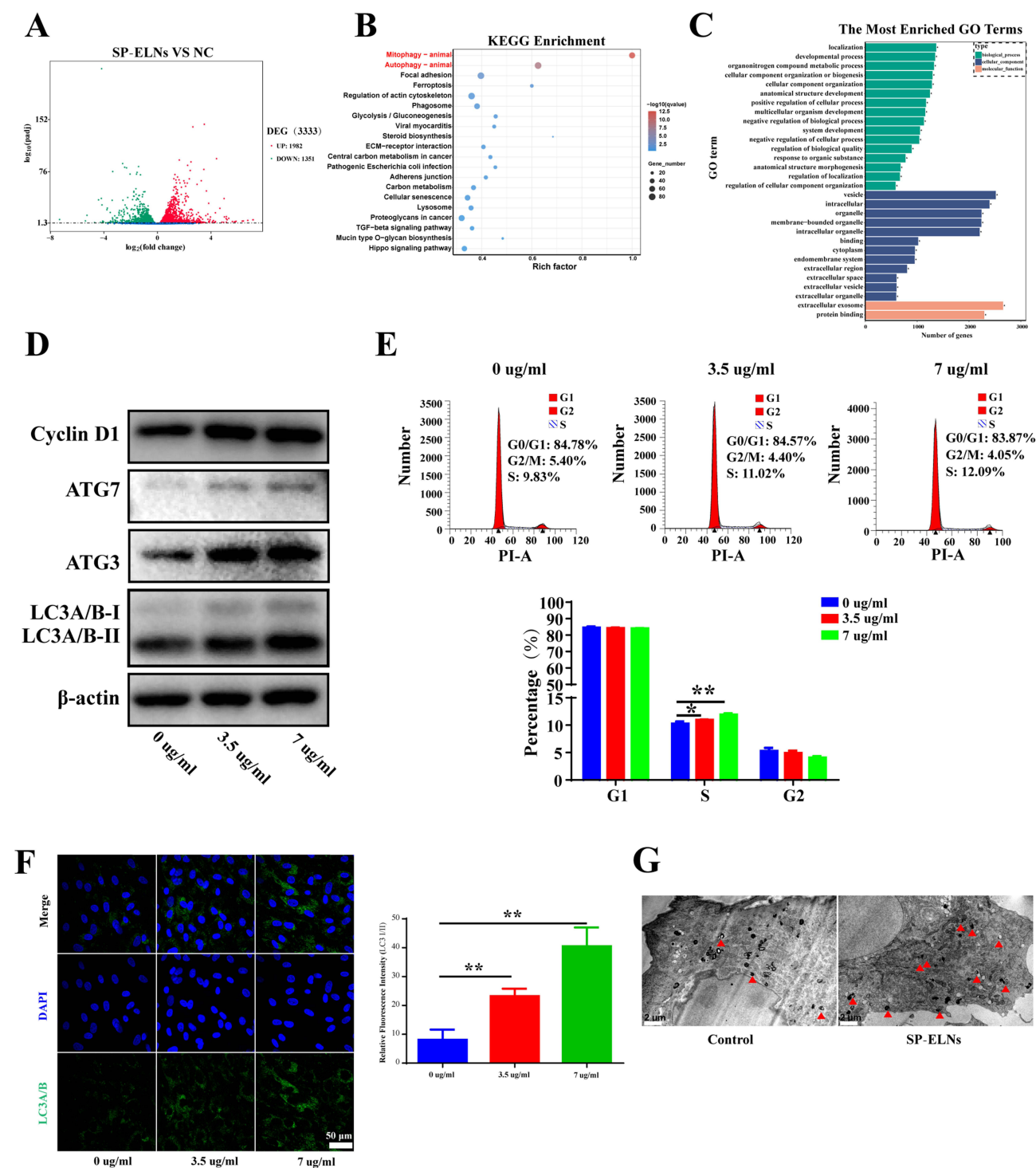


**Figure 3** SP-EVLP promoted cell cycle and autophagy. **(A)** A volcano plot was constructed to graphically represent the DEGs between the control and SP-EVLP treated groups. **(B-C)** KEGG and GO analysis analyses were performed to elucidate the pathways and biological functions associated with the DEGs. **(D)** Western blotting was employed to assess the protein expression levels of autophagy-related proteins (ATG3, ATG7, and LC3 I/II) and the cell cycle-related protein (Cyclin D1). **(E)** Cell cycle progression was analyzed using flow cytometry. **(F)** Immunofluorescence microscopy was utilized to visualize the distribution of the autophagy-related protein LC3 I/II (green) within the cells, with nuclei counterstained by DAPI (blue). **(G)** Transmission electron microscopy (TEM) was employed to observe the formation of autophagosomes. The red arrows denote the autophagic vacuoles. Data represent means  $\pm$  SD at least 3 separate experiments. \* $P < 0.05$ , and \*\* $P < 0.01$ .

upregulation of autophagy markers ATG3, ATG7, and the conversion of LC3 I to LC3 II (Figure 3D). Immunofluorescence staining revealed elevated LC3 puncta in SP-EVLP-treated cells (Figure 3F), and TEM also demonstrated more autophagic vacuoles after the administration of SP-EVLP (Figure 3G), suggesting increased

autophagosome formation. These data suggest that SP-EVLP promote osteogenic differentiation in hBMSCs through the activation of autophagy.

## Suppressing Autophagy Inhibits the Osteogenic Differentiation by SP-EVLP

To ascertain the role of autophagy in SP-EVLP-induced osteogenesis, hBMSCs were incubated with 3-methyladenine (3-MA, 0.25  $\mu$ M) to suppress autophagy. ALP activity (Figure 4A, down) and ARS staining (Figure 4A, up) indicated that 3-MA co-treatment markedly decreased these osteogenic indicators compared to SP-EVLP treatment alone. Western blotting confirmed downregulation of ALP and RUNX2 in the presence of 3-MA (Figure 4B). Moreover, 3-MA abrogated SP-EVLP-induced autophagy, evidenced by reduced levels of ATG3, ATG7, and LC3 I-to-II conversion (Figure 4C). Correspondingly, immunofluorescence staining showed diminished RUNX2 expression with 3-MA co-treatment (Figure 4D). Additionally, immunofluorescence corroborated these findings, with decreased LC3 I/II puncta upon 3-MA co-treatment (Figure 4E). Collectively, these data underscore the indispensable function of autophagy in the osteogenic effects of SP-EVLP on hBMSCs.

## SP-EVLP Prevented Ovariectomy-Induced Bone Loss

Given the susceptibility of exosomes to gastric acid degradation,<sup>28</sup> we utilized enteric-coated capsules for the intestinal delivery of SP-EVLP (SP-EVLP@Cap). The capsules remained intact in acidic environments for over 120 minutes and dissolved completely within 30 minutes in intestinal fluid (Figure 5A). To track bone tissue accumulation, SP-EVLP were labeled with DiR and orally administered to rats; DiR signals were detected in bones, heart, livers, kidneys, and intestines, confirming bone accumulation (Figure 5B). Over time, SP-EVLP were metabolized and cleared from the rat.

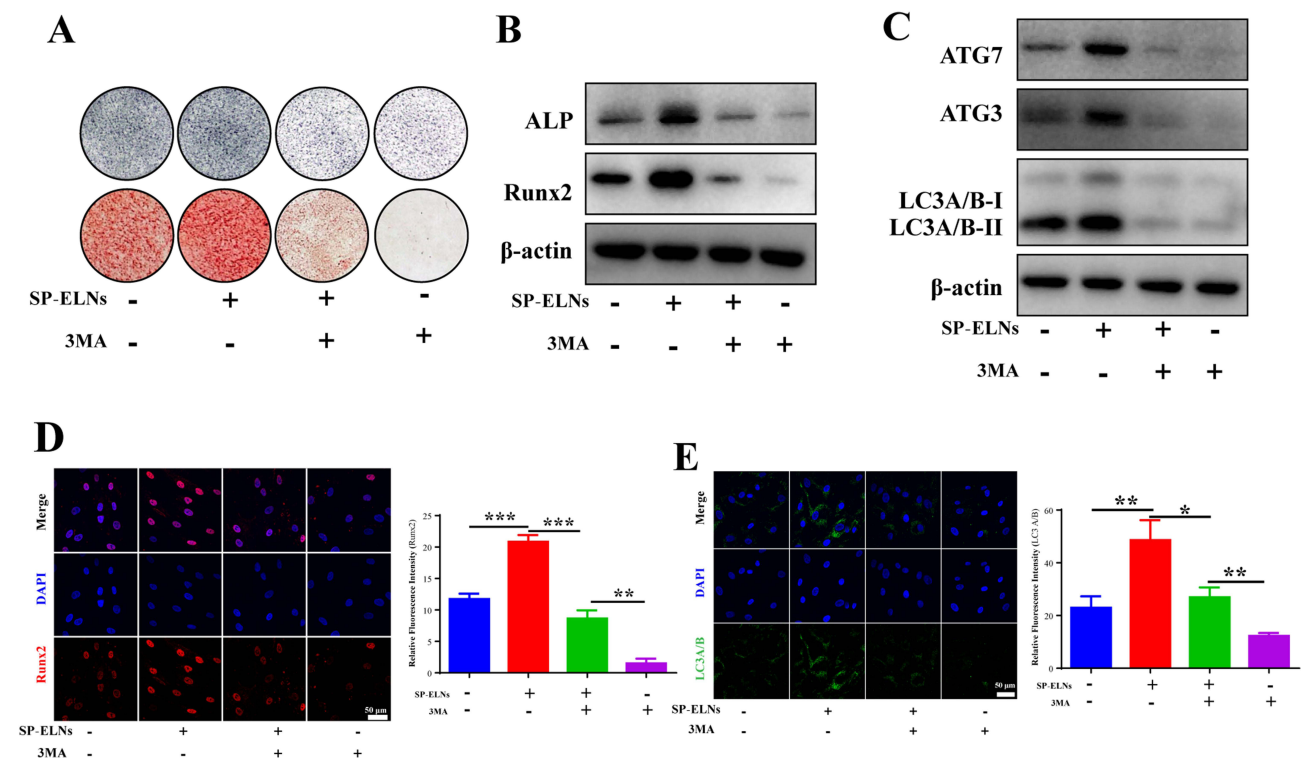


**Figure 4** Suppressing autophagy inhibits the osteogenic differentiation by SP-EVLP. **(A)** ALP activity and ARS staining were performed to evaluate the osteogenic differentiation of hBMSCs treated with 3MA (0.5  $\mu$ M) or SP-EVLP (7  $\mu$ g/mL) for 3 and 14 days, respectively. **(B)** Western blot analysis was used to examine the expression levels of ALP and RUNX2 after the treatment of 3MA or SP-EVLP. **(C)** Western blot analysis was conducted to assess the expression levels of ATG3, ATG7 and LC3 I/II after the administration of 3MA or SP-EVLP. **(D)** Immunofluorescence microscopy was employed to visualize the intracellular localization of RUNX2 (red), with nuclei stained by DAPI (blue). **(E)** Immunofluorescence imaging was utilized to observe the distribution of the LC3 I/II (green), with nuclei counterstained by DAPI (blue). Data represent means  $\pm$  SD at least 3 separate experiments. \* $P < 0.05$ , \*\* $P < 0.01$ , and \*\*\* $P < 0.001$ .

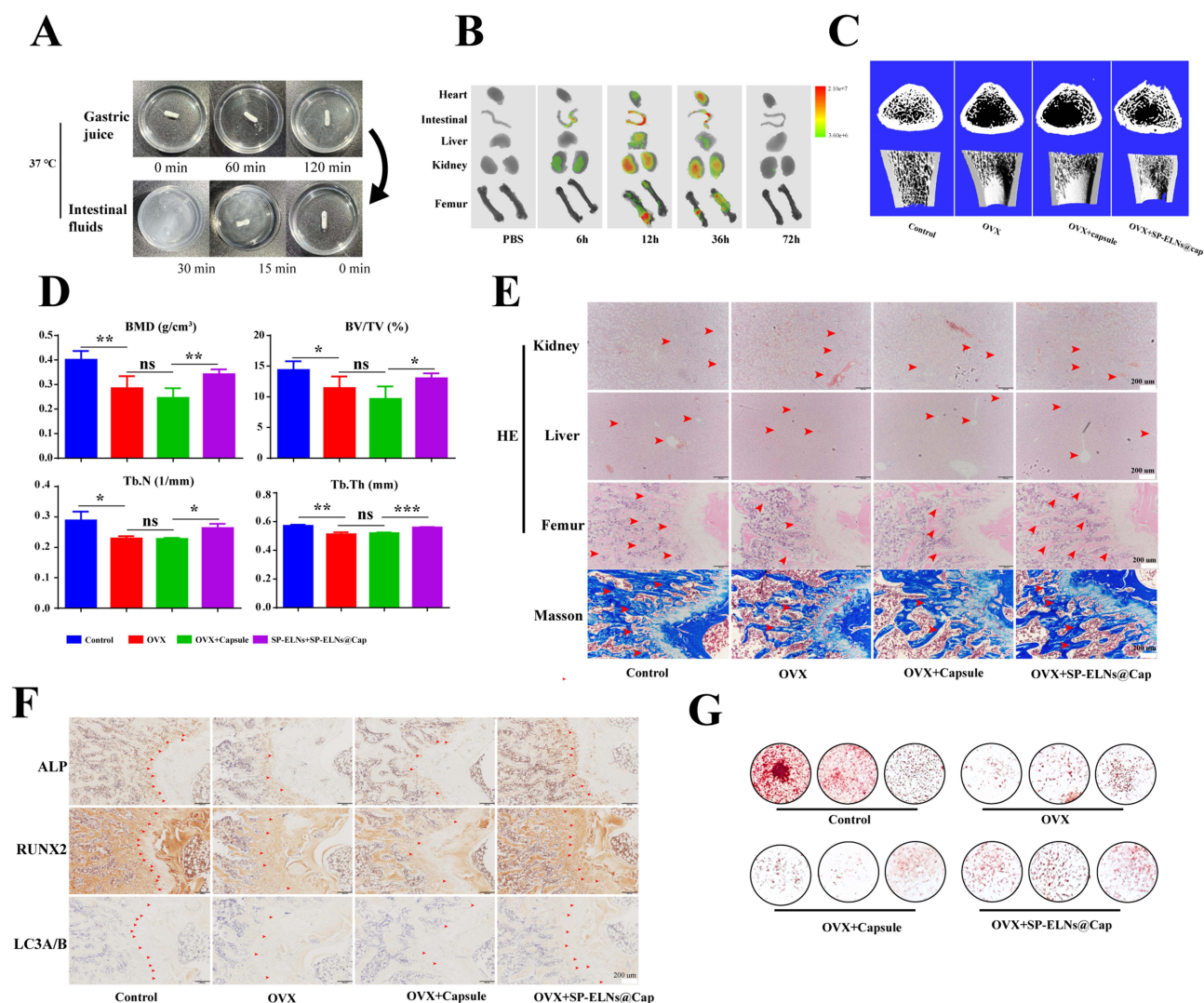


**Figure 5** SP-EVLP prevented ovariectomy-induced bone loss. **(A)** The structural integrity of SP-EVLP@Cap when exposed to acidic conditions and the degradation in the intestinal fluid. **(B)** Images of the intestine, liver, kidneys, heart, and femurs were captured at 6, 12, 36, and 72 hours post-oral administration of DiR-labeled SP-EVLP@Cap to assess the biodistribution and tissue interaction. The micro-CT images **(C)**, BV/TV and BMD analysis **(D)** of femurs from in SD rat by treatment with SP-EVLP@Cap. **(E)** Hepatotoxicity and nephrotoxicity were observed by HE staining in SD rat after the administration of SP-EVLP@Cap. In addition, representative photographs of H&E and Masson's trichrome staining of osteocalcin in femurs treated with SP-EVLP@Cap were also shown. The red arrows denote the renal glomeruli, hepatic lobules, and trabecular bone, respectively. **(F)** IHC staining of ALP, RUNX2 and LC3II in rat femur paraffin sections after the treatment of SP-EVLP@Cap. The red arrows denote the positive cells in the immunohistochemical assays. **(G)** The ARS staining was performed to evaluate the osteogenic differentiation on rBMSCs derived from the rats of these four groups. Data represent means  $\pm$  SD at least 3 separate experiments. \* $P < 0.05$ , and \*\* $P < 0.01$ .

An osteoporosis rat model was established via ovariectomy, and the impact of SP-EVLP@Cap on bone loss was examined. Micro-CT analysis showed reduced trabecular bone loss in treated OVX rat compared to the control group, with no protective effect observed for Cap alone (Figure 5C). Treatment with SP-EVLP@Cap increased bone regeneration markers, such as BMD, BV/TV, Tb.N and Tb.Th, which were decreased in the OVX group (Figure 5D). After 8 weeks of oral gavage treatment with SP-EVLP@Cap, no hepatotoxicity or nephrotoxicity was observed by H&E staining (Figure 5E). Consistent with the micro-CT findings, H&E staining showed higher trabecular number in the SP-EVLP@Cap group (Figure 5E). Masson staining also suggested significantly osteopenic phenotypes in the OVX group, which was reversed after the administration of SP-EVLP@Cap. Immunohistochemistry revealed increased ALP and RUNX2 expression in the SP-EVLP@Cap-treated group, indicating elevated osteoblastic activity. Additionally, higher expression levels of autophagy marker LC3II were observed, suggesting enhanced autophagy (Figure 5F). Moreover, compared to the OVX group, SP-EVLP@Cap treatment significantly promoted osteogenic differentiation of rat bone



osteogenesis and alleviate osteoporosis by modulating autophagy via melatonin, which providing an innovative therapeutic to treat osteoporosis effectively while minimizing adverse outcomes.

Extracellular vesicles (EVs), specifically exosomes, have emerged as novel approach to regulate bone homeostasis.<sup>32</sup> Their systemic administration and bone tissue accumulation, attributed to their small size and bone matrix affinity, overcome the limitations of traditional treatments, such as side effects and poor targeting specificity.<sup>33</sup> They also facilitate sustained delivery of anabolic factors, enhancing bone formation over resorption. Exosome-like nanoparticles from natural sources, such as *Pueraria*<sup>12</sup> and *yam*,<sup>11</sup> have shown therapeutic potential in osteoporosis. Additionally, nanoparticles from the medicinal insect *Periplaneta americana* L have demonstrated efficacy in accelerating wound healing.<sup>34</sup> *Steleophaga plancyi* (Boleny) has been noted for its use in treating cancer and bone-related diseases.<sup>19</sup> Our experiments have shown that SP-EVLP are effectively internalized by hBMSCs, promoting their osteogenic differentiation. In vivo studies confirm that SP-EVLP accumulate in bone tissue and mitigate bone loss in the OVX rat model of osteoporosis. Furthermore, SP-EVLP enhance hBMSCs' proliferation and cell cycle progression, highlighting their potential in regulating osteogenic differentiation.

Volcano plot and GO/KEGG analyses of RNA data indicate that SP-EVLP enhance osteogenic activity by modulating autophagy pathways. Increasing evidence suggests that autophagy plays a fundamental role in the progression of pathological osteoporosis due to the correlation between autophagy and bone physiology.<sup>35</sup> Autophagy has been correlated with MSCs stemness and osteogenic differentiation.<sup>36</sup> Our findings show that SP-EVLP upregulate autophagy markers ATG3, ATG7, and LC3 II in hBMSCs. Conversely, 3-MA treatment downregulates osteogenic markers such as ALP activity, mineralization, and RUNX2 expression compared to SP-EVLP alone. This suggests that SP-EVLP stimulate osteoblast differentiation and mineralization by regulating autophagy.

Melatonin, a hormone integral to circadian rhythm regulation, has emerged as a significant factor in osteogenic differentiation and bone health.<sup>37</sup> Our study identified melatonin as a crucial metabolite in BMSCs treated with SP-EVLP. The exogenous application of melatonin significantly enhanced ALP and ARS staining. Furthermore, melatonin treatment upregulated the expression of ALP and RUNX 2. Drawing from the human endogenous metabolite database, we noted that melatonin is implicated in the modulation of the autophagy signaling pathway. Western blot analysis substantiated this by demonstrating upregulated expression of ATG7 and ATG3, alongside the conversion of LC3 from LC3I to LC3II. These findings underscore the role of melatonin in promoting osteogenic differentiation through the activation of autophagy, thereby enhancing the osteogenic potential of BMSCs.

Stomach acid can degrade exosomes, impairing their structure and function.<sup>28</sup> To avoid this, we employed enteric-coated capsules designed to transport SP-EVLP directly to the intestines.<sup>38</sup> These capsules are stable in acidic conditions but rapidly dissolve in the intestine. To assess the potential systemic side effects of orally ingested SP-EVLP, a dosage of 10 mg/kg every three days for 8 weeks were given to OVX rat via oral gavage. Throughout the treatment period and post-treatment, the rat remained in good health, with no significant alterations in body weight, behavior, or feeding habits ([supplementary Figure 1](#)). Histological examination of liver and kidney tissues via H&E staining revealed no signs of damage attributable to SP-EVLP. Collectively, these findings suggest that oral administration of SP-EVLP is devoid of adverse effects.

## Conclusion

In summary, the extraction, purification, and characterization of SP-EVLP were achieved with success. SP-EVLP were found to enhance the growth, differentiation, and mineralization of osteoblasts by melatonin-modulated autophagy. When delivered orally, SP-EVLP traversed the gastrointestinal tract and were absorbed in the small intestine. SP-EVLP notably boosted bone formation in a rat model of postmenopausal osteoporosis induced by ovariectomy. Furthermore, no hepatic or renal toxicity was detected following 8 weeks of SP-EVLP treatment. Consequently, SP-EVLP emerges as a promising therapeutic candidate for osteoporosis management, exhibiting superior biocompatibility and safety profiles.

## Data Sharing Statement

The original contributions presented in the study are included in the article/[Supplementary Material](#). Further inquiries can be directed to the corresponding authors.

## Compliance with Ethics Requirements

All experimental procedures with rat were approved by the Institutional Animal Care and Use Committee of the Affiliated Hospital of Guangdong Medical University (AHGDMU-LAC-B-202404-0021) and used in line with the NIH Guide for the Care and Use of Laboratory Animals.

## Funding

This research was funded by the Guangdong and Enterprises Joint Fund of Public Health and Medicine Area, China (2022A1515220054), Science and Technology Program of Zhanjiang, China (2021A05069), Special fund for Affiliated Hospital of Guangdong Medical University “Clinical Medicine +” CnTech Co-construction Platform (CLP2021A001), Discipline Construction Project of Guangdong Medical University (4SG24001G), Open funding of Affiliated Hospital of Guangdong Medical University-Research of autophagy and diseases.

## Disclosure

The authors declare no conflicts of interest.

## References

1. Ensrud KE, Crandall CJ. Osteoporosis. *Ann Intern Med.* 2017;167:ITC17–ITC32. doi:10.7326/AITC201708010
2. Deardorff WJ, Cenzler I, Nguyen B, Lee SJ. Time to benefit of bisphosphonate therapy for the prevention of fractures among postmenopausal women with osteoporosis: a meta-analysis of randomized clinical trials. *JAMA Intern Med.* 2022;182(1):33–41. doi:10.1001/jamainternmed.2021.6745
3. Johnston CB, Dagar M. Osteoporosis in Older Adults. *Med Clin North Am.* 2020;104(5):873–884. doi:10.1016/j.mcna.2020.06.004
4. Jiang Y, Zhang P, Zhang X, Lv L, Zhou Y. Advances in mesenchymal stem cell transplantation for the treatment of osteoporosis. *Cell Prolif.* 2021;54:e12956 doi:10.1111/cpr.12956
5. Aibar-Almazan A, Voltas-Martinez A, Castellote-Caballero Y, Afanador-Restrepo DF, Carcelen-Fraile MDC, Lopez-Ruiz E. Current status of the diagnosis and management of osteoporosis. *Int J mol Sci.* 2022;23(16):9465. doi:10.3390/ijms23169465
6. Karimi SM, Bayat M, Rahimi R. Plant-derived natural medicines for the management of osteoporosis: a comprehensive review of clinical trials. *J Tradit Complement Med.* 2024;14(1):1–18. doi:10.1016/j.jtcme.2023.08.001
7. Lai JJ, Chau ZL, Chen SY, et al. Exosome processing and characterization approaches for research and technology development. *Adv Sci.* 2022;9:e2103222 doi:10.1002/adv.202103222
8. Lu J, Chen J, Ye J, et al. Dipsacus asperoides-derived exosomes-like nanoparticles inhibit the progression of osteosarcoma via activating P38/JNK signaling pathway. *Int J Nanomed.* 2024;19:1097–1108. doi:10.2147/IJN.S446594
9. De Robertis M, Sarra A, D’Oria V, et al. Blueberry-derived exosome-like nanoparticles counter the response to tnf-alpha-induced change on gene expression in EA.hy926 cells. *Biomolecules.* 2020;10 doi:10.3390/biom10050742
10. Leiva-Sabadini C, Alvarez S, Barrera NP, Schuh C, Aguayo S. Antibacterial effect of honey-derived exosomes containing antimicrobial peptides against oral streptococci. *Int J Nanomed.* 2021;16:4891–4900. doi:10.2147/IJN.S315040
11. Hwang JH, Park YS, Kim HS, et al. Yam-derived exosome-like nanovesicles stimulate osteoblast formation and prevent osteoporosis in mice. *J Control Release.* 2023;355:184–198. doi:10.1016/j.jconrel.2023.01.071
12. Zhan W, Deng M, Huang X, et al. Pueraria lobata-derived exosome-like nanovesicles alleviate osteoporosis by enhancing autophagy. *J Control Release.* 2023;364:644–653. doi:10.1016/j.jconrel.2023.11.020
13. Meng F, Xue X, Yin Z, Gao F, Wang X, Geng Z. Research progress of exosomes in bone diseases: mechanism, diagnosis and therapy. *Front Bioeng Biotechnol.* 2022;10:866627. doi:10.3389/fbioe.2022.866627
14. Salimi L, Akbari A, Jabbari N, et al. Synergies in exosomes and autophagy pathways for cellular homeostasis and metastasis of tumor cells. *Cell Biosci.* 2020;10(1):64. doi:10.1186/s13578-020-00426-y
15. Van den Broek B, Pintelon I, Hamad I, et al. Microglial derived extracellular vesicles activate autophagy and mediate multi-target signaling to maintain cellular homeostasis. *J Extracell Vesicles.* 2020; 10:e12022 doi:10.1002/jev2.12022
16. Tian L, Jin J, Lu Q, et al. Bidirectional modulation of extracellular vesicle-autophagy axis in acute lung injury: molecular mechanisms and therapeutic implications. *Biomed Pharmacother.* 2024;180:117566. doi:10.1016/j.biopha.2024.117566
17. Yang X, Song X, Li Z, Liu N, Yan Y, Liu B. Crosstalk between extracellular vesicles and autophagy in cardiovascular pathophysiology. *Pharmacol Res.* 2021;172:105628. doi:10.1016/j.phrs.2021.105628
18. Kim BS, Jin S, Park JY, Kim SY. Scoping review of the medicinal effects of Eupolyphaga sinensis walker and the underlying mechanisms. *J Ethnopharmacol.* 2022;296:115454. doi:10.1016/j.jep.2022.115454
19. Fu X, Shao BH, Wei X, et al. Tubiechong:A review on ethnomedicinal uses, bioactive chemical constituents and pharmacological activities. *J Ethnopharmacol.* 2022;298:115642. doi:10.1016/j.jep.2022.115642

20. Peng LW, Yang HX. Effect of *Eupolyphaga sinensis walker* on mandibular distraction osteogenesis in rabbits. *Zhonghua Zheng Xing Wai Ke Za Zhi*. 2013;29(2):125–130 doi:10.3760/cma.j.issn.1009-4598
21. Park SB, Kim CH, Hong M, Yang HJ, Chung CK. Effect of a selective estrogen receptor modulator on bone formation in osteoporotic spine fusion using an ovariectomized rat model. *Spine J*. 2016;16(1):72–81. doi:10.1016/j.spinee.2015.08.061
22. Zhu WY, Yang WF, Wang L, et al. The effect of drug holiday on preventing medication-related osteonecrosis of the jaw in osteoporotic rat model. *J Orthop Translat*. 2023;39:55–62. doi:10.1016/j.jot.2022.12.006
23. Shuid AN, Ping LL, Muhammad N, Mohamed N, Soelaiman IN. The effects of *Labisia pumila var. alata* on bone markers and bone calcium in a rat model of post-menopausal osteoporosis. *J Ethnopharmacol*. 2011;133(2):538–542. doi:10.1016/j.jep.2010.10.033
24. Hu Y, Hou Z, Liu Z, et al. Oyster mantle-derived exosomes alleviate osteoporosis by regulating bone homeostasis. *Biomaterials*. 2024;311:122648. doi:10.1016/j.biomaterials.2024.122648
25. Wiklander OP, Nordin JZ, O’Loughlin A, et al. Extracellular vesicle in vivo biodistribution is determined by cell source, route of administration and targeting. *J Extracell Vesicles*. 2015;4(1):26316. doi:10.3402/jev.v4.26316
26. Hu J, Jiang Y, Wu X, et al. Exosomal miR-17-5p from adipose-derived mesenchymal stem cells inhibits abdominal aortic aneurysm by suppressing TXNIP-NLRP3 inflammasome. *Stem Cell Res Ther*. 2022;13(1):349. doi:10.1186/s13287-022-03037-1
27. Lee H, Kim SHL, Yoon H, et al. Intracellular delivery of recombinant RUNX2 facilitated by cell-penetrating protein for the osteogenic differentiation of hMSCs. *ACS Biomater Sci Eng*. 2020;6(9):5202–5214. doi:10.1021/acsbomaterials.0c00827
28. Cheng Y, Zeng Q, Han Q, Xia W. Effect of pH, temperature and freezing-thawing on quantity changes and cellular uptake of exosomes. *Protein Cell*. 2019;10(4):295–299. doi:10.1007/s13238-018-0529-4
29. Al Saedi A, Sharma S, Summers MA, Nurgali K, Duque G. The multiple faces of tryptophan in bone biology. *Exp Gerontol*. 2020;129:110778. doi:10.1016/j.exger.2019.110778
30. Hawarden A, Paskins Z, Mughal F. What’s new in osteoporosis management? Leading the fight in primary care. *Br J Gen Pract*. 2024;74(747):472–475. doi:10.3399/bjgp24X739641
31. Brown JP. Long-term treatment of postmenopausal osteoporosis. *Endocrinol Metab*. 2021;36(3):544–552. doi:10.3803/EnM.2021.301
32. Yu B, Gao Q, Sheng S, et al. Smart osteoclasts targeted nanomedicine based on amorphous CaCO<sub>3</sub> for effective osteoporosis reversal. *J Nanobiotechnol*. 2024;22(1):153. doi:10.1186/s12951-024-02412-9
33. Shan SK, Lin X, Li F, et al. Exosomes and Bone Disease. *Curr Pharm Des*. 2019;25(42):4536–4549. doi:10.2174/1381612825666191127114054
34. Liao Q, Su L, Pang L, et al. Natural exosome-like nanoparticles derived from ancient medicinal insect *Periplaneta americana* L. as a novel diabetic wound healing accelerator. *J Nanobiotechnology*. 2023;21(1):169. doi:10.1186/s12951-023-01923-1
35. Wang J, Zhang Y, Cao J, et al. The role of autophagy in bone metabolism and clinical significance. *Autophagy*. 2023;19(9):2409–2427. doi:10.1080/15548627.2023.2186112
36. Zhang L, Zheng YL, Wang R, Wang XQ, Zhang H. Exercise for osteoporosis: a literature review of pathology and mechanism. *Front Immunol*. 2022;13:1005665. doi:10.3389/fimmu.2022.1005665
37. Munmun F, Witt-Enderby PA. Melatonin effects on bone: implications for use as a therapy for managing bone loss. *J Pineal Res*. 2021; 71:e12749 doi:10.1111/jpi.12749
38. Miller DS, Parsons AM, Bresland J, et al. A simple and inexpensive enteric-coated capsule for delivery of acid-labile macromolecules to the small intestine. *J Zhejiang Univ Sci B*. 2015;16(7):586–592. doi:10.1631/jzus.B1400290

International Journal of Nanomedicine

Publish your work in this journal

The International Journal of Nanomedicine is an international, peer-reviewed journal focusing on the application of nanotechnology in diagnostics, therapeutics, and drug delivery systems throughout the biomedical field. This journal is indexed on PubMed Central, MedLine, CAS, SciSearch®, Current Contents®/Clinical Medicine, Journal Citation Reports/Science Edition, EMBase, Scopus and the Elsevier Bibliographic databases. The manuscript management system is completely online and includes a very quick and fair peer-review system, which is all easy to use. Visit <http://www.dovepress.com/testimonials.php> to read real quotes from published authors.

Submit your manuscript here: <https://www.dovepress.com/international-journal-of-nanomedicine-journal>

**Dovepress**  
Taylor & Francis Group